

Giant Voltage Enhancement *via* Triboelectric Charge Supplement Channel for Self-Powered Electroadhesion

Liang Xu,^{†,§,#} Hao Wu,^{‡,#} Guo Yao,^{‡,#} Libo Chen,^{†,§} Xiaodan Yang,^{†,§} Baodong Chen,^{†,§} Xin Huang,[‡] Wei Zhong,^{†,§} Xiangyu Chen,^{*,†,§} Zhouping Yin,^{*,‡} and Zhong Lin Wang^{*,†,§,||}

[†]CAS Center for Excellence in Nanoscience, Beijing Key Laboratory of Micro-nano Energy and Sensor, Beijing Institute of Nanoenergy and Nanosystems, Chinese Academy of Sciences, Beijing, 100083, People's Republic of China

[‡]Flexible Electronics Research Center, School of Mechanical Science and Engineering, Huazhong University of Science and Technology, Wuhan, Hubei 430074, People's Republic of China

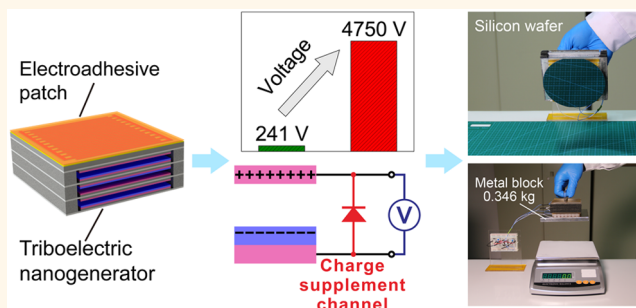
[§]School of Nanoscience and Technology, University of Chinese Academy of Sciences, Beijing, 100049, People's Republic of China

^{||}School of Material Science and Engineering, Georgia Institute of Technology, Atlanta, Georgia 30332, United States

Supporting Information

ABSTRACT: Electroadhesion generates an adhesion force using an externally applied power source, which has versatile applications in robotics and material handling. In this study, a self-powered electroadhesion system using enhanced triboelectric nanogenerators (TENGs) to supply power for electroadhesion is presented. By introducing a triboelectric charge supplement channel, the open circuit voltage of the TENG can be significantly boosted by over 10 times, from ~230 V to more than 3300 V for a single TENG unit, providing sufficiently high voltage for an electroadhesive patch to generate enough adhesion for practical use. The charge supplement channel takes effect through a replenishing mechanism for dissipated charges, maintaining an optimal charge distribution throughout TENG electrodes, which enables the highest open circuit voltage under given surface charge density and device configuration. The fabricated self-powered electroadhesion system shows the ability to manipulate objects of various materials *via* easy and straightforward operations, demonstrating a great potential for applications in material handling and robotics. Moreover, the voltage enhancement mechanism by the charge supplement channel could be extended to TENGs of other modes, which can provide reliable power sources for various applications that require a high voltage.

KEYWORDS: charge supplement, voltage enhancement, triboelectric nanogenerator, electroadhesion, self-powered



Electroadhesion is a promising adhesion mechanism for robotics and material handling.^{1–3} An electroadhesive patch (EAP) consists of a set of electrodes and an insulating layer. Through applying high voltage on the electrodes, electroadhesive force between the electrodes and the substrate can be generated by high electric field induced polarization (when the substrate is nonconductive) or electrostatic induction (when the substrate is conductive).^{4,5} Electroadhesion was first used in the semiconductor industry, such as in chemical vapor deposition (CVD) and etching systems,⁶ and its potential applications have recently been extended to robots, such as wall climbing robots,⁷ perching robots,² or even soft robotic actuators.³ Compared with conventional adhesion mechanisms such as chemical, magnetic, or pneumatic adhesion, electroadhesion has the advantages of high adaptability to various substrate materials,

gentle/flexible handling, and low energy consumption.⁸ However, a key drawback of electroadhesion is that the system requires an externally applied high-voltage (usually on the scale of a few thousand volts) power supply, which induces system complexity and high cost and limits its practical use in various prospective scenarios such as emerging robotic systems.^{2,9} Thus, seeking an advanced power source is crucial for further development of the electroadhesion system.

Triboelectric nanogenerators (TENGs), which can effectively convert ambient mechanical energy into electricity based on triboelectrification and electrostatic induction, could be an

Received: July 16, 2018

Accepted: September 6, 2018

Published: September 6, 2018

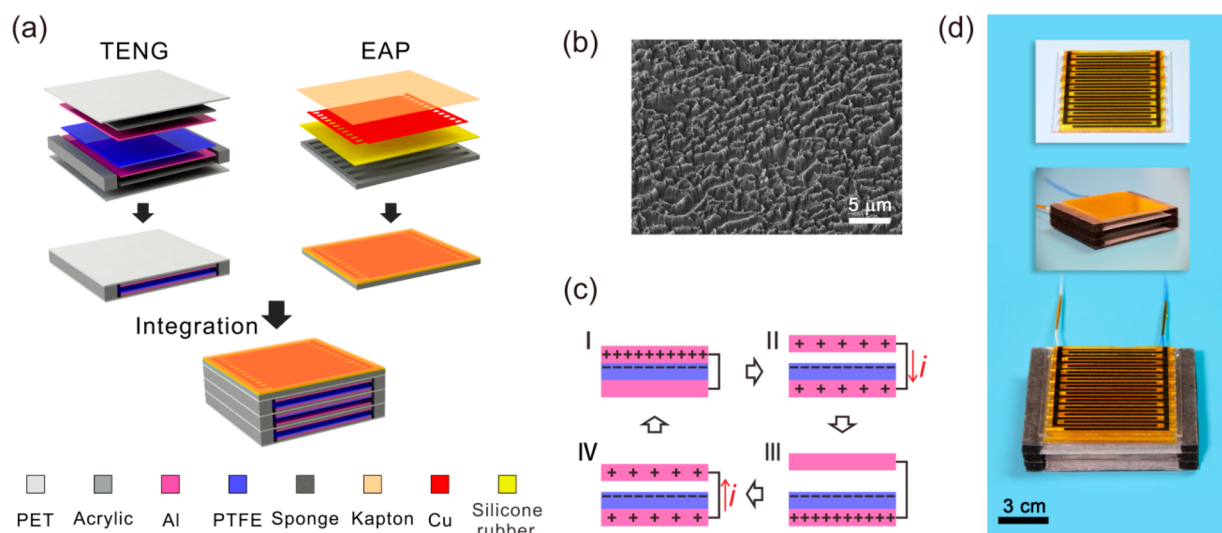


Figure 1. Structure design of the self-powered electroadhesion system. (a) Integration process of the system from three triboelectric nanogenerators (TENGs) and one electroadhesive patch (EAP) (not to scale). (b) SEM image of the etched nanostructures on the PTFE surface. (c) Basic working principle of the TENG (not to scale). (d) Photograph of the fabricated system. Insets show the EAP and the stacked TENGs, respectively.

ideal candidate to meet such a demand because of its high output voltage.^{10,11} Since their invention in 2012, significant research efforts have been devoted to optimizing the performance of the TENG and promoting its applications.^{12–17} Due to outstanding properties such as versatile material options, simple structure, easy and scalable fabrication, and low cost,^{18,19} the TENG has been adopted to harvest energy from wind,²⁰ water waves,^{21–24} and human motion.^{25,26} Meanwhile, the TENG also provides a platform for the construction of self-powered sensory devices such as tactile sensors,^{27,28} accelerometers,²⁹ vibration sensors,³⁰ and so on. Especially, based on its characteristic of high voltage output, the TENG was demonstrated to drive high-voltage devices,^{31,32} rendering its feasibility in powering electroadhesion systems. In principle, by harvesting energy from the environment and converting it into high-voltage electricity, the TENG could drive the EAP directly, imparting desired features to electroadhesion systems, such as self-powering, light weight, and even flexibility and stretchability with certain materials.^{25,26} However, challenges still remain. An ultrahigh voltage of a few thousand volts is usually only available for TENGs of specific modes, such as the single-electrode mode or the freestanding triboelectric-layer mode with small internal impedance, and corona charging or severe rubbing to enhance the surface charge density and large device size are usually required.³³ Thus, great efforts are still needed to develop a reliable high voltage output with convenient and straightforward operations for the application of TENGs in electroadhesion systems.

In this study, a self-powered electroadhesion system by effectively integrating contact–separation mode TENGs and an electroadhesive patch is presented. To achieve the requirement of electroadhesion, a charge supplement channel (CSC) is proposed for boosting the open circuit voltage of the TENG. Such CSC can provide a replenishing mechanism for dissipated charges, then maintain the optimal charge distribution state throughout TENG electrodes, which enables the highest open circuit voltage under a given surface charge density and device configuration. A giant voltage enhancement

of over 10 times and a voltage value of 7000 V are obtained by TENGs with the supplement channel, providing an effective power supply for the generation of electroadhesion. Based on the boosted voltage of the TENG, the self-powered electroadhesion system can handle and manipulate objects of conductive, semiconductive, and nonconductive materials *via* easy and straightforward operations. The enhanced TENG with a high-voltage capacitor shows effective generation of high voltage output while attenuating its rapid decay, demonstrating an economical and practical solution to promote widespread applications of a TENG as a high-voltage power supply.

RESULTS AND DISCUSSION

The self-powered electroadhesion system consisting of three TENG units and an electroadhesive patch is illustrated in Figure 1a. The contact–separation mode is adopted for the TENGs since its operation is consistent with the adhesion and release process of the EAP, which facilitates straightforward control and status monitoring of the overall electroadhesion system. An aluminum foil is chosen as one tribolayer and top electrode, while a polytetrafluoroethylene (PTFE) thin film is employed as the other tribolayer and another Al foil is adhered to the back side of the PTFE film as the counter electrode. The contact and separation motions of the TENGs are realized by applying forces and the rebound enabled by the sponge and poly(ethylene terephthalate) (PET) sheet, respectively. Figure 1b shows a scanning electron microscopy (SEM) image of the PTFE thin film, which was treated by dry etching to create nanostructures to enhance the triboelectrification effect.^{34,35} More details on the fabrication procedures of TENGs are provided in the Experimental Section. The EAP unit is composed of a Kapton insulating film, interdigitated electrodes, a silicone encapsulation layer, and an acrylic support structure, and the fabrication process of EAP is illustrated in Figure S1 in the Supporting Information. The layout of the interdigitated electrodes is shown in Figure S2 (Supporting Information), with two key parameters, electrode width h and gap width w . The dimensions of the whole interdigitated electrodes are 70 mm × 70 mm. The optical photographs of

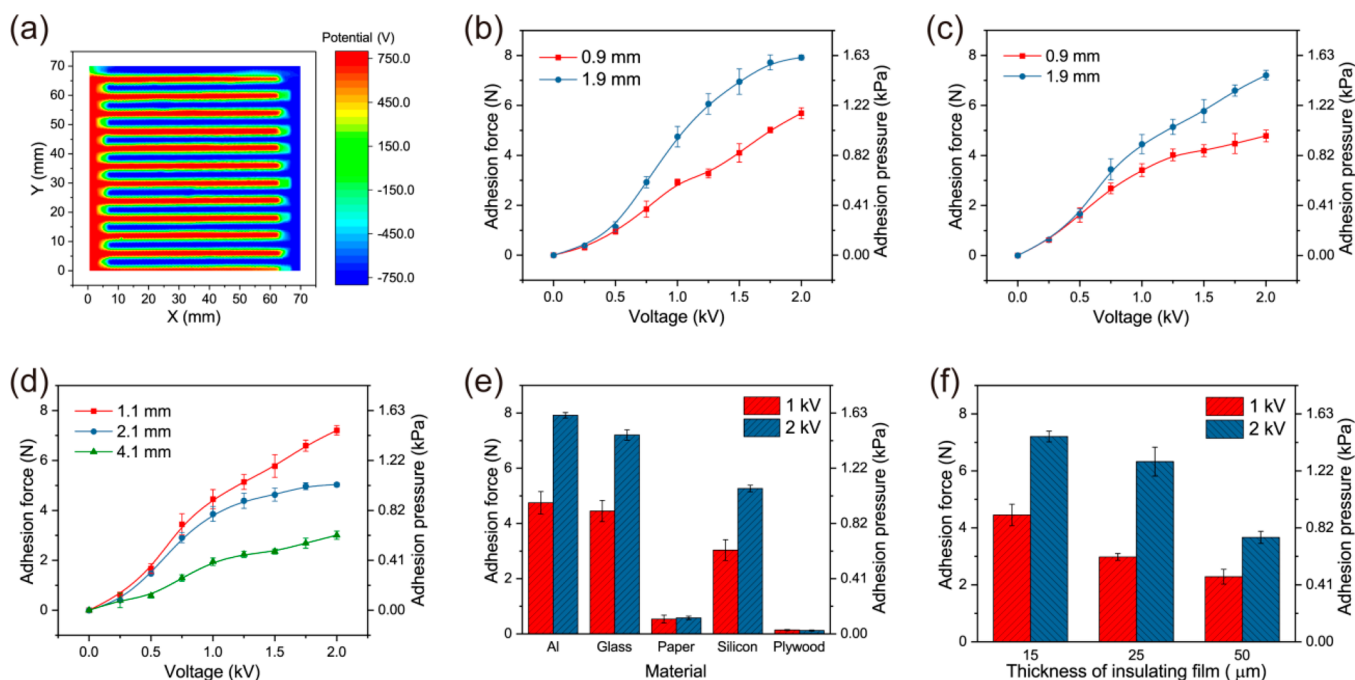


Figure 2. Adhesion performance of the EAP powered by a commercial voltage source. (a) Measured surface potential distribution of the EAP under a voltage of 1500 V. (b–f) Adhesion force and pressure of the EAP on different substrates: (b) different voltages and electrode widths on an Al plate, (c) different voltages and electrode widths on glass, (d) different voltages and gap widths on glass, (e) different substrate materials and voltages, and (f) different thicknesses of insulating film and voltages. The EAP electrode width is 1.9 mm, the electrode gap is 1.1 mm, and the thickness of the insulating film is 15 μm , unless otherwise specified.

the integrated self-powered electroadhesion system consisting of TENGs and EAP are presented in Figure 1d.

The fundamental working principle of the TENG, which is based on the conjugation of triboelectrification and electrostatic induction, is illustrated in Figure 1c. When the PTFE layer is brought into contact with the top Al layer, due to their difference in triboelectric series, the surface of the PTFE layer would be negatively charged and the Al layer would be positively charged. Then during the separation process, the negative charges on the PTFE surface would induce lower electric potential on the back side Al electrode through electrostatic induction, resulting in the transfer of positive charges from the top Al electrode to the back side Al electrode and electric current in the external circuit. When the Al and PTFE layers approach each other and eventually contact again, the negative charges on the PTFE surface would induce lower potential on the top Al layer, leading to current flow in the reverse direction. In this manner, the TENG outputs alternating electric signals through periodic contact–separation motion of the tribolayers.

As discussed earlier, the EAP unit can realize adhesion to various substrate materials due to electrostatic attraction force generated between opposite charges on the EAP and the substrate surface. More specifically, when a high voltage V is applied to the interdigitated electrodes of the EAP, reverse charges will be induced on the contact area for a conductive substrate, leading to attractive forces; for substrates of nonconductive materials, the reverse surface charges are induced by electric field induced polarization, as illustrated in Figure S3 (Supporting Information). The surface electric potential of the EAP upon application of voltage was measured, as shown in Figures 2a and S6 (Supporting Information). It is noted that the EAP surface potential distribution is consistent with the geometric pattern of the

interdigitated electrodes, and the potential difference of the two regions agrees with the magnitude of the voltage applied. The electric field E for inducing reverse charges on substrates can be deduced by the differentiation of potential:

$$E = -\nabla V \quad (1)$$

To quantitatively characterize the performance of the EAP, adhesion forces were measured by applying different voltages. A commercial voltage source was adopted for stable and accurate measurements of the correlation between applied voltage and adhesion force, and schematics of the electric circuit and experimental setup are shown in Figures S4 and S5 (Supporting Information), respectively. Briefly, the EAP was put into contact with the substrate and then powered by the voltage source through a rectifier until reaching a certain level of voltage. Afterward, the switch in the circuit was turned off and the EAP was lifted until separation between the EAP and the substrate occurred. The lifting force was measured through a load cell, and the adhesion force is defined as the peak value of the lifting force subtracted by the weight of the EAP, as illustrated in Figure S7 in the Supporting Information. In order to prevent rapid decay of the input voltage after switching off the power supply, a 10 nF capacitor was parallel connected to the EAP in the measurement circuit. More details of the experiments can be found in the Experimental Section.

Figure 2b and c show the adhesion forces between the EAP and aluminum or glass substrates with different EAP electrode widths. To prevent electrical breakdown, adhesion forces by voltages of no more than 2000 V were tested. It is noted that the adhesion force increases monotonically as the input voltage rises. The EAP with electrode width $h = 1.9$ mm yields larger force than that with $h = 0.9$ mm under the same condition. At 2000 V, the EAP can generate an adhesion force as large as 7.92 N or a pressure of 1.62 kPa on aluminum plates, while

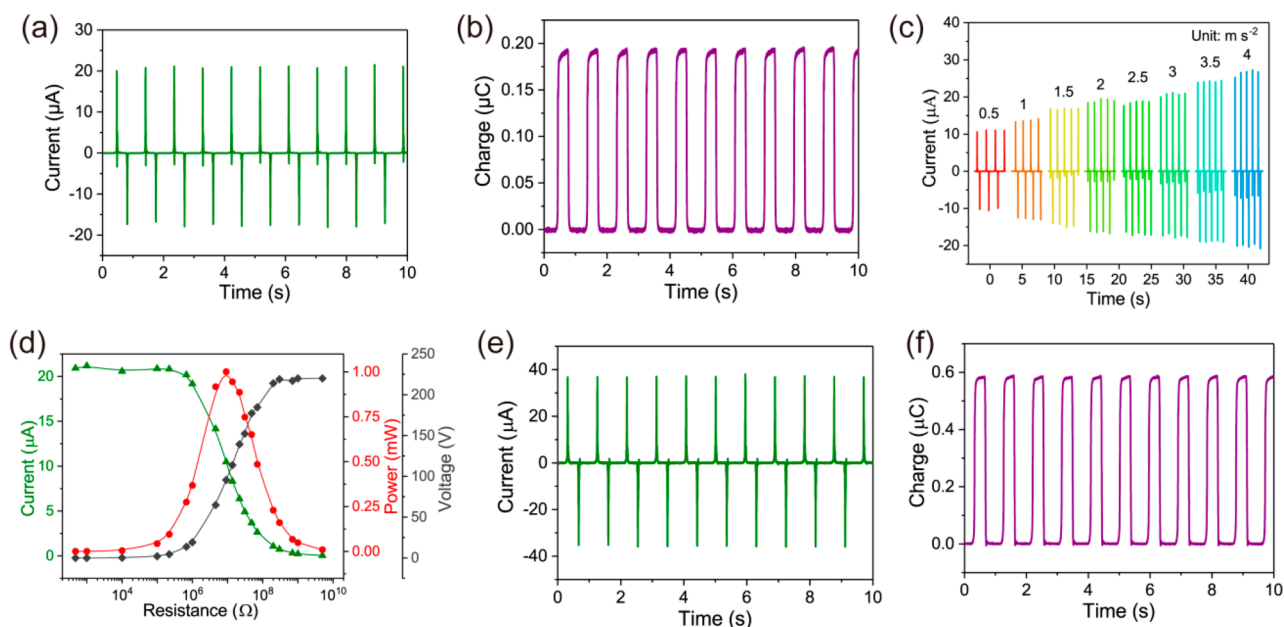


Figure 3. Electrical output characterization of the TENG. (a, b) Short circuit current and transferred charges of a single TENG unit. (c) Short circuit current under different accelerations of the contact–separation motion of a single TENG. (d) Dependence of peak power, peak current, and peak voltage on the load resistance for a single TENG. (e, f) Short circuit current and transferred charges of three TENGs in parallel.

adhesion on glass substrates is slightly lower, reaching 7.21 N or 1.47 kPa. Figure 2d illustrates that the increase of the electrode gap w leads to lower adhesion force. The above results are consistent with theoretical predictions and experimental results in literature reports.⁴ A variety of substrate materials were tested, and it was found that the EAP yields higher adhesion on dense materials such as Al, silicon, and glass than on loose or porous materials including paper and plywood (Figure 2e). The thickness of the Kapton insulating film on the EAP surface significantly affects the magnitude of the electric field for the same applied voltage. Figure 2f shows an intuitive trend that the decrease of such thickness can contribute to higher adhesion force. Through the systematic tests above, it is clear that the EAP is capable of generating satisfactory adhesion on substrates of various materials with enough voltage supply.

The performance of the TENG was also evaluated, as shown in Figure 3. A linear motor was used to drive the contact and separation motion of the tribolayers of the TENG for accurate and repeatable motion control. Figure 3a and b show the short circuit current and transferred charges of a single TENG unit, which reach 21 μA and 0.19 μC , respectively, under a motion acceleration of 3 m s^{-2} . The increase of acceleration leads to an almost linear rise of short circuit current (Figure 3c). Figure 3d demonstrates the dependence of output peak voltage, peak current, and peak power on load resistance, and the maximum power is about 1 mW when the resistance is 9.13 M Ω . Parallel integration of three TENG units can enhance the transferred charges and short circuit current, as shown in Figure 3e and f. The amount of transferred charges can be boosted to 0.58 μC , and the short circuit current can be enhanced to 37 μA .

When using TENGs as the power supply for the EAP, the amount of transferred charges and the open circuit voltage are two crucial parameters. This is because the EAP has similar electric characteristics to a capacitor, with a capacitance of 23 pF in this study. Thus, the increase rate of the voltage in the

EAP is affected by the amount of transferred charges of TENGs, while the maximum achievable voltage applied to the EAP is determined by the open circuit voltage of the TENGs. Here, the requirement for the amount of transferred charges can be satisfied by parallel connection of multiple TENGs with enhanced output, as shown in Figure 3f. For the voltage, as shown in Figure 3d, a single TENG unit can provide a voltage of about 220 V at high resistance (which is close to the open circuit voltage), and parallel connection of multiple TENGs will not greatly improve the output voltage. In fact, open circuit voltage of contact–separation mode TENGs is typically measured to be only a few hundred volts,³⁶ which is much lower than required to drive the EAP for electroadhesion. To solve this issue, we propose a mechanism to significantly boost the open circuit voltage to thousands of volts. This approach can be easily implemented through parallel connection of a high-voltage diode to the TENG output port, with the anode of the diode connecting to the back side Al electrode of the TENG. The diode can act as a charge supplement channel, which can replenish charges to the electrodes. The TENG with the CSC is illustrated in Figure 4a. To demonstrate the effect of the CSC, we measured the open circuit voltage of a single TENG unit with and without the CSC, where a positive voltage represents higher potential in the top Al electrode relative to the back side Al electrode. The results are shown in Figure 4b. It can be observed that the peak of the voltage with the CSC can reach as high as more than 3300 V, and the voltage is maintained as non-negative, indicating that the top Al electrode keeps a potential not lower than the back side Al electrode. When the CSC is withdrawn from the circuit, the open circuit voltage sharply declines and negative voltage appears; eventually the positive peak of the voltage becomes stable at about 230 V. It is clear that the adoption of the CSC provides a 14-fold enhancement of voltage output. Figure 4c further presents the dependence of the peak open circuit voltage on the separation distance of a CSC-enhanced TENG.

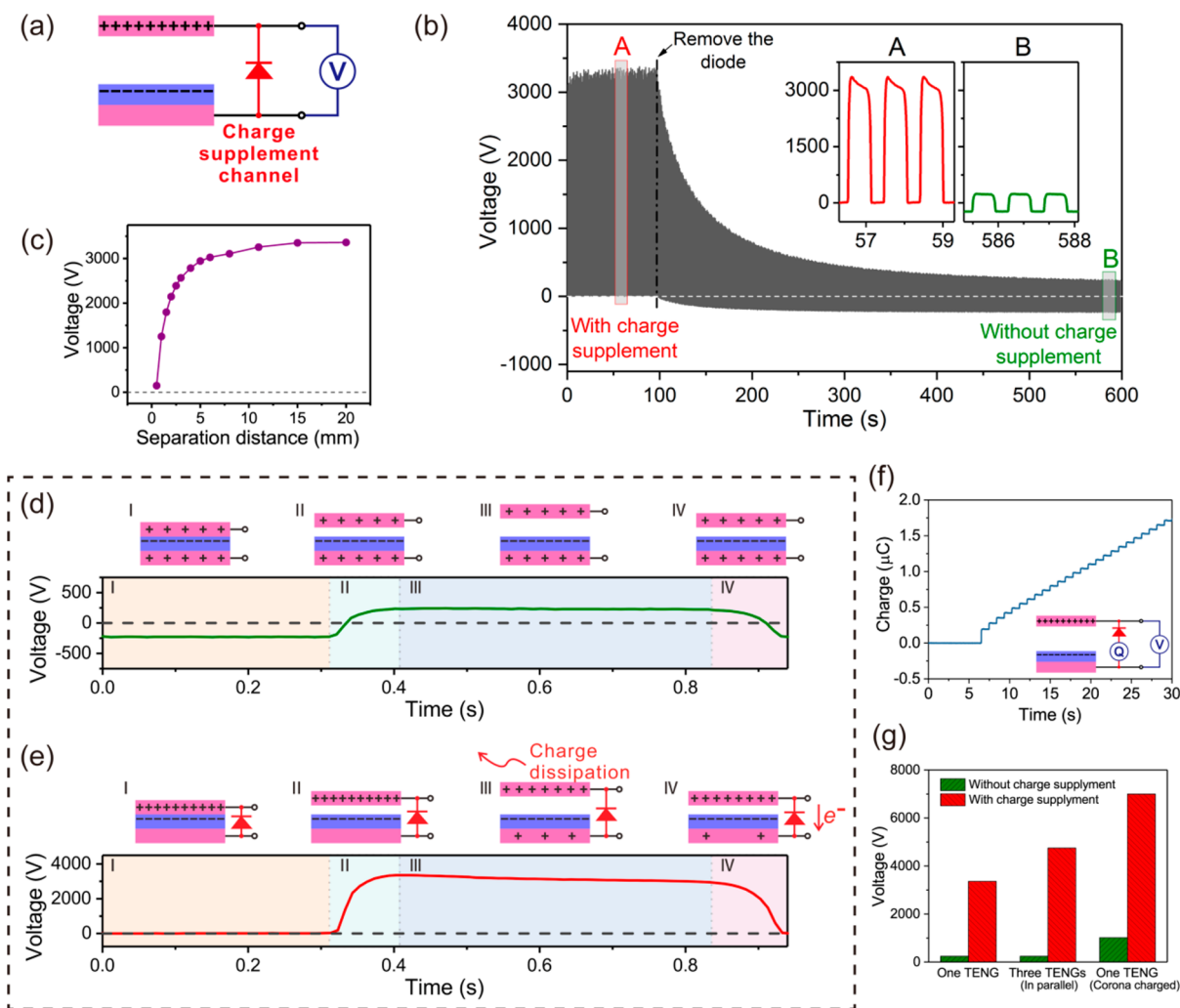


Figure 4. Giant voltage enhancement *via* the charge supplement channel. (a) Schematic diagram of the charge supplement channel. (b) Comparison of open circuit voltage of the TENG with and without charge supplement by removing the supplement diode. Insets show corresponding details of the voltage. (c) Dependence of open circuit voltage on separation distance with charge supplement. (d, e) Comparison of voltage output processes for TENGs with (e) and without (d) charge supplement and working mechanism of the charge supplement channel. (f) Supplemented charges *via* the channel. Inset shows the measurement setup. (g) Voltage enhancement for different TENG systems.

The voltage rises rapidly with increasing separation distance, and a distance of merely 5 mm is needed for the open circuit voltage to approach the high plateau value.

In order to fully understand the voltage-boosting mechanism of the CSC, in-depth analysis on the influential factors of TENG open circuit voltage is required. Besides the well-known factors such as material, structure, and surface charge density, another important point that has been usually neglected is the charge distribution in the electrodes. To illustrate this point, the expression of the voltage of contact–separation mode TENG is given as³⁷

$$V_{\text{TENG}} = -\frac{Q}{S\epsilon_0}(d_0 + x(t)) + \frac{\sigma x(t)}{\epsilon_0} \quad (2)$$

For the case of this study, Q is the charge amount in the back side electrode; S is the effective area of the TENG; σ is the absolute value of the surface charge density of the PTFE film; ϵ_0 is the dielectric constant of the vacuum; $x(t)$ is the separation distance; d_0 is the effective thickness of the PTFE film, defined as the actual thickness d divided by the relative

dielectric constant of PTFE ϵ_r . A corresponding illustration of these parameters is shown in Figure S8 in the Supporting Information. Besides, the charge amount of the top Al electrode can be calculated as $S\sigma - Q$ to maintain electric neutrality of the system. While in the open circuit state, eq 2 also expresses the open circuit voltage V_{OC} of the TENG. It is clear that Q plays an important role in determining the open circuit voltage. Only under the condition that $Q = 0$ can the open circuit voltage reach a maximum achievable value of $\sigma x(t)/\epsilon_0$, which is the generally discussed theoretical open circuit voltage before,³⁷ and the voltage during the whole contact–separation cycle is always non-negative. When Q is a positive value, the peak open circuit voltage may drop significantly and a negative value will appear in the voltage curve. In addition, a negative Q is not possible according to the working mechanism of the TENG. The above discussion also indicates one important reason for the observation that the measured open circuit voltage of TENGs is often lower than the theoretical prediction of $\sigma x(t)/\epsilon_0$,^{11,38} as the practical charge distribution in the electrodes does not always meet the zero Q hypothesis underlying the theory. According to eq 2,

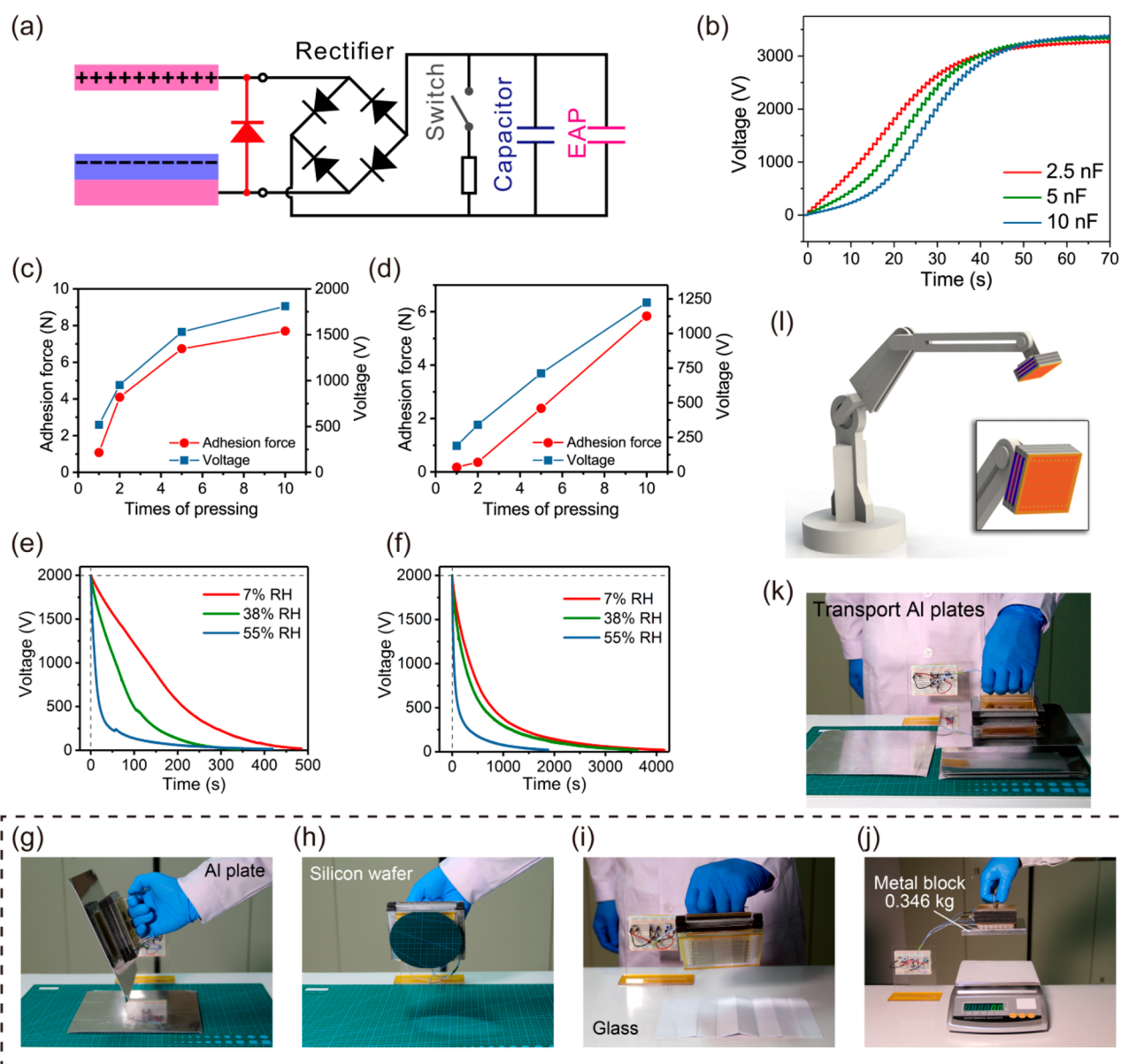


Figure 5. Self-powered electroadhesion system for various applications. (a) Schematic diagram of the application circuit. (b) Charging different capacitors to high voltage. (c, d) Adhesion force and voltage achieved by different times of pressing on Al plates without a capacitor (c) and with a 2.5 nF capacitor (d), respectively. (e, f) Voltage decay of the EAP under different relative humidity without capacitor (e) and with a 10 nF capacitor (f), respectively. (g–j) Photographs of the self-powered electroadhesion system handling Al plate, silicon wafer, glass, and metal block, respectively. (k) Photograph of the self-powered electroadhesion system transporting Al plates. (l) Imaginary picture of a robot arm with the self-powered electroadhesion system. Inset shows the system details.

curves A and B in Figure 4b can be regarded as in different charge distribution states, and a gradual increase of Q occurs when the CSC is absent, resulting in the decline of peak open circuit voltage. As the TENG is in an open circuit state, such charge variation cannot be realized through an external circuit, but most probably is caused by charge dissipation from a high electrode potential,³⁹ which will be further discussed later. Generally speaking, with the CSC, the variation of charge distribution under high voltage is suppressed, and the peak open circuit voltage can be sustained at a much higher level. Otherwise, the charge distribution would change gradually under high voltage, and it eventually leads to low voltage output as usually reported in the literature.³⁶

To explicitly reveal the mechanism for the CSC to suppress variation of charge distribution, a comparison of the evolution

of charge distribution and voltage output of the TENG without and with the CSC is shown in Figure 4d and e, respectively. For the situation with the CSC shown in Figure 4e, a TENG working cycle can be divided into four phases. At phase I, the top Al electrode contacts the PTFE film, which is negatively charged at the surface, and the top Al electrode is positively charged with all the positive charges, resulting in $Q = 0$ at this stage. Since the positive and negative charges are physically close to each other, their influences on the electric potential of the surroundings will cancel out; thus there is almost zero voltage between the top Al electrode and the back side Al electrode. At phase II, the voltage between the top and back side Al electrodes increases as the separation distance between the two tribolayers increases, which drives the diode to the cutoff state. When the separation distance reaches around the

maximum at phase III, the voltage rises to above 3000 V. Such high voltage leads to charge dissipation from the top electrode and thereby voltage attenuation, as can be observed from the slow decline of the voltage curve in Figure 4e.³⁹ Meanwhile, due to the high electric field induced by the negative static charges on the PTFE surface, a similar charge dissipation effect also occurs, which is realized by increasing positive charges on the back side Al electrode that can partly attenuate the electric field caused by the negative charges. In such a case, Q will have a value larger than zero. At phase IV, the voltage declines as the top Al electrode approaches the PTFE. According to eq 2, there exists a Q -related threshold distance below which the voltage will become negative, and the diode will switch into the conducting state with charge transfer occurring through the diode, supplementing positive charges to the top electrode until the two tribolayers contact. Once the two tribolayers come into contact again, the charge supplement *via* the CSC completes and the system returns to phase I with $Q = 0$. It can be observed that the output voltage of the TENG is maintained as non-negative throughout the four phases above. In comparison, for the working cycles of a regular contact–separation mode TENG without a CSC, charge dissipation will also occur at high voltage, but no supplement mechanism exists. Thus, even if initially positive charges only distribute in the top Al electrode, the charge distribution of the system will transit gradually to reach the illustrated quasi-stable state in Figure 4d, and gradual accumulation of positive charges on the back side Al electrode will cause a decline in peak output voltage, similar to the situation shown in Figure 4b after the diode is removed. In the four phases of the TENG without a CSC at quasi-stable state shown in Figure 4d, due to the presence of positive charges on the back side Al electrode, the output voltage alternates between positive and negative values with low peaks while the contact and separation motions cycle. As can be inferred from the above discussion, the adoption of the diode provides a voltage-controlled charge supplement channel. Once charge dissipation between the electrodes occurs, the voltage near the contact state would change to negative, which can activate the channel to supplement charges. Therefore, the variation of Q can be suppressed in each period and the output voltage can be maintained at a high level.

The transferred charges across the CSC during the contact–separation operation of the TENG were measured to verify the charge supplement mechanism proposed above, as shown in Figure 4f. It is observed that the amount of supplemented charges increases monotonically, which implies that the flow of charges through the CSC is in a single direction, consistent with the proposed supplement mechanism. This also indicates the charge dissipation during phase III does not largely occur through reverse leakage of the diode; otherwise the amount of transferred charges will demonstrate nonmonotonic variation.

In addition to a single TENG, the CSC can also be effectively applied to other configurations of TENG devices, as shown in Figure 4g. The voltage of three TENG units in parallel can be increased from 240 V to 4700 V by the adoption of the CSC, and the CSC can boost the output of a corona-charged single TENG unit from 1000 V to 7000 V.³³ Indeed, even higher voltage can be expected through the CSC, and the challenge of application will lie primarily on compatible designs of the materials and devices to prevent breakdown under high voltage.

With the enhancement of the CSC, the voltage of the TENG unit is capable of driving the EAP to work effectively. An application circuit was designed as shown in Figure 5a. The TENG with the CSC is connected to the EAP through a rectifier, and a high-voltage capacitor and a switch are connected parallel to the EAP. The capacitor can enable stable adhesion for a long period by slowing down the attenuation of the high voltage on the EAP, and the release of the adhesion can be realized through turning on the switch. Figure 5b shows the charging performance of a CSC-enhanced TENG to different capacitors. It is observed that the capacitors can be charged to more than 3000 V in tens of seconds, while they can only be charged to about 300 V by a TENG without a CSC (Figure S9 in the Supporting Information). Due to the much lower capacitance of the EAP, the voltage can ramp up more quickly when charged. The voltage and adhesion force generated by the fully integrated self-powered electroadhesion system consisting of three CSC-enhanced TENGs and the EAP (shown in Figure 1d) upon pressing are illustrated in Figure 5c and d. Without capacitors in the circuit (Figure 5c), the voltage of the EAP can reach more than 1500 V quickly before the buildup slows down, and the corresponding adhesion force demonstrates a similar trend. After five times of pressing the TENGs, the voltage can go up to about 1500 V with 6.7 N adhesion force generated. Integration of a 2.5 nF capacitor in the circuit slows down the rise of voltage and adhesion force, where the output voltage and adhesion can still reach about 1200 V and 5.8 N, respectively, after 10 times of pressing the TENGs (Figure 5d).

Figure 5e and f present the decay of the EAP voltage at various relative humidity (RH) values without and with capacitors, respectively. It is noted that the EAP voltage declines quickly and the decay rate rises as the humidity increases without capacitors. With a 10 nF capacitor (Figure 5f), the decay rate of voltage is significantly reduced. At a medium relative humidity of 38%, it takes about 600 s for the voltage of 2000 V to decrease to 500 V, while the same amount of reduction happens in only about 100 s if the circuit does not integrate the capacitor. It is clear that the capacitor in the circuit can maintain a longer period of high voltage; however, the choice of capacitance has to be considered carefully to achieve balance since large capacitance will slow down the buildup of high voltage. The utility of the integrated self-powered electroadhesion system is demonstrated through pickup, manipulation, and transport of conductive, semi-conductive, and nonconductive materials, as shown in Figure 5g–k and Videos S1–S4 in the Supporting Information. By a single pressing operation, light objects such as aluminum plates and silicon wafers can be handled, while pressing twice enables pickup and manipulation of glass plates, and a 0.35 kg metal block can be picked up after five times of pressing the device. The release of objects can be realized by simply turning on the switch to create a short circuit for EAP electrodes. Through those demonstrations, it is clear that the implementation of the CSC in TENGs can effectively power adhesion force generation in the EAP for practical applications. The advantages of this self-powered electroadhesion system include light weight, low material cost, easy and economical approach for achieving high voltage, and straightforward operation by simply pressing on the surface of substrates. Such self-powered electroadhesion system is promising for applications in mobile robots, robotic manipulators, and semiconductor manufactur-

ing systems. Figure S1 shows an imaginary robot arm with the self-powered electroadhesion system.

The voltage enhancement mechanism by the CSC proposed in this study should not be limited to contact–separation mode TENGs, and it could also be effective for other modes of TENGs theoretically. Through integration with energy storage devices, the CSC-enhanced TENGs provide a highly effective and economical solution for high voltage generation, with great prospects for widespread applications in areas including microfluidics, dielectric elastomer and artificial muscle actuation, *etc.*^{31,32,40,41}

CONCLUSIONS

In this work, a self-powered electroadhesion system constructed through integration of contact–separation mode TENGs and an electroadhesive patch is reported. A triboelectric charge supplement channel is proposed to boost the open circuit voltage of the TENG to achieve the requirement of electroadhesion. By providing a replenishing mechanism for dissipated charges, the charge supplement channel can maintain an optimal charge distribution throughout TENG electrodes, which enables the highest open circuit voltage under a given surface charge density and device configuration. For TENGs without the supplement channel, such a charge distribution state is not stable and usually decays rapidly with low voltage output. A giant voltage enhancement of over 10 times and a voltage value of 7000 V are obtained by TENGs with the supplement channel. Based on the boosted voltage of the TENG, the self-powered electroadhesion system achieves adhesion forces to manipulate objects of conductive, semi-conductive, and nonconductive materials *via* easy and straightforward operations, demonstrating great potential for applications in material handling and robotics. Moreover, the charge supplement channel should be a universal strategy for enhancing the open circuit voltage of different types of TENGs, and the integrated system consisting of TENGs with the charge supplement channel and a high-voltage capacitor can effectively generate high voltage output and attenuate its rapid decay, providing an economical and practical solution for various application scenarios where high-voltage power supply is required.

EXPERIMENTAL SECTION

Fabrication and Integration of the TENG and the EAP. A PTFE thin film of 50 μm thickness was cleaned, and a layer of Cu sputtered. Then inductively coupled plasma (ICP) reactive ion etching (SENTECH/SI-500) was applied to fabricate nanostructures on the PTFE surface. Specifically, O_2 , Ar, and CF_4 gases were introduced into the ICP chamber with flow rates of 10.0, 15.0, and 30.0 sccm (standard cubic centimeter per minute), respectively. A power of 400 W was used to generate a large density of plasma, and another power of 100 W was used to accelerate the plasma ions. The etching time was about 6 min. Afterward, the PTFE film with nanostructures was cut into pieces with a size of 80 mm \times 80 mm, and a thin Al foil, an acrylic plate, and a PET thin plate (85 mm \times 105 mm) were adhered to the backside in sequence. Another component was fabricated similarly, by adhering an Al foil, an acrylic plate, and a PET thin plate together. A TENG unit was constructed by bonding the two PET plates through two strips of sponge with the PTFE and the Al foil facing each other.

The fabrication of the EAP is illustrated in Figure S1 (Supporting Information). A piece of adhesive paper on release paper was laser scribed to create the reversal image pattern of the interdigitated electrodes, and the rest of the adhesive paper was stripped off. Afterward, the scribed adhesive paper was transferred to a Kapton film

(75 mm \times 75 mm) as a mask. Then, the surface of the Kapton film was sputtered a thin adhesion layer of Cr, followed by a layer of Cu (Denton Vacuum/Discovery 635). The Cu sputtering lasted 30 min with a power of 100 W. Then the mask was stripped off and a layer of silicone rubber was spin coated onto the surface for encapsulation. Finally, the EAP was achieved by bonding the structure to an acrylic substrate as support.

The structure of the self-powered electroadhesion system was integrated by simply bonding three TENGs and the EAP together with adhesives.

Measurement of the Adhesion Force. As shown in Figures S4 and S5 (Supporting Information), for the adhesion force powered by a commercial voltage source, the EAP unit was placed on a substrate with a certain voltage for 1 min to reach stable equilibrium; then the switch connecting the voltage source was turned off and the EAP was lifted until separation between the EAP and the substrate occurred. The lifting force was recorded by a force gauge (Handpi/HP-10), and the adhesion force is defined as the peak value of the lifting force subtracted by the weight of the EAP (Figure S7 in the Supporting Information). Afterward, the EAP was put on hold for 6 min to dissipate residual electrostatic charges before the next measurement, where the direction of the voltage was reversed. By reversing voltage direction alternately, excessive polarization of dielectric materials in the EAP can be suppressed.^{2,40}

Electrical Measurement. The open circuit voltage was measured by an electrostatic voltmeter (Trek 344) with a divider for the ultrahigh voltage test, and the relative humidity was controlled in the range of 30–38%. The surface potential of the EAP was measured by surface scanning with the voltmeter probe. The short circuit current and transferred charges were measured by an electrometer (Keithley 6514). A diode of type 2CL70 was used as the CSC for most experiments.

ASSOCIATED CONTENT

Supporting Information

The Supporting Information is available free of charge on the ACS Publications website at DOI: 10.1021/acsnano.8b05359.

Figures of the fabrication process of the EAP; geometric layout of the EAP electrodes; schematic illustration of the electroadhesion mechanism; schematic diagram of the circuit to power EAP by a commercial voltage source; experiment setup for the measurement of adhesion force; surface potential distribution of the EAP in three-dimensional view; profile of the measured adhesion force; theoretical model of the TENG; charging performance of the TENG without charge supplement for different capacitors (PDF)

Video S1: Handling and transport of Al plates by the self-powered electroadhesion system (AVI)

Video S2: Handling and manipulation of a silicon wafer by the self-powered electroadhesion system (AVI)

Video S3: Pickup of a glass plate by the self-powered electroadhesion system (AVI)

Video S4: Comparison of the self-powered electroadhesion system with and without charge supplement to pick up a heavy metal block (AVI)

AUTHOR INFORMATION

Corresponding Authors

*E-mail: chenxiangyu@binn.cas.cn.

*E-mail: yinzhp@mail.hust.edu.cn.

*E-mail: zlwang@binn.cas.cn.

ORCID

Zhong Lin Wang: 0000-0002-5530-0380

Author Contributions

[#]L. Xu, H. Wu, and G. Yao contributed equally to this work.

Notes

The authors declare no competing financial interest.

ACKNOWLEDGMENTS

We would like to thank J. Luo for taking SEM images of the nanostructures. The research was supported by the National Key R & D Project from Minister of Science and Technology, China (2016YFA0202704), National Natural Science Foundation of China (Grant Nos. 51605033, 51735001, 91648115, and 51432005), the “Thousands Talents” Program for Pioneer Researcher and His Innovation Team, China, the “Thousands Talents” Program for Young Professionals, China, China Postdoctoral Science Foundation (Grant No. 2015M581041), and Beijing Municipal Science & Technology Commission (Grant No. Z171100000317001).

REFERENCES

- (1) Monkman, G. J. An Analysis of Astrictive Prehension. *Int. J. Robot. Res.* **1997**, *16*, 1–10.
- (2) Graule, M. A.; Chirarattananon, P.; Fuller, S. B.; Jafferis, N. T.; Ma, K. Y.; Spenko, M.; Kornbluh, R.; Wood, R. J. Perching and Takeoff of a Robotic Insect on Overhangs Using Switchable Electrostatic Adhesion. *Science* **2016**, *352*, 978–982.
- (3) Shintake, J.; Rosset, S.; Schubert, B.; Floreano, D.; Shea, H. Versatile Soft Grippers with Intrinsic Electro-adhesion Based on Multifunctional Polymer Actuators. *Adv. Mater.* **2016**, *28*, 231–238.
- (4) Guo, J.; Bamber, T.; Chamberlain, M.; Justham, L.; Jackson, M. Optimization and Experimental Verification of Coplanar Interdigital Electro-adhesives. *J. Phys. D: Appl. Phys.* **2016**, *49*, 415304.
- (5) Ruffatto, D.; Parness, A.; Spenko, M. Improving Controllable Adhesion on Both Rough and Smooth Surfaces with a Hybrid Electrostatic/Gecko-Like Adhesive. *J. R. Soc., Interface* **2014**, *11*, 20131089.
- (6) Asano, K.; Hatakeyama, F.; Yatsuzuka, K. Fundamental Study of an Electrostatic Chuck for Silicon Wafer Handling. *IEEE Trans. Ind. Appl.* **2002**, *38*, 840–845.
- (7) Liu, R.; Chen, R.; Shen, H.; Zhang, R. Wall Climbing Robot Using Electrostatic Adhesion Force Generated by Flexible Interdigital Electrodes. *Int. J. Adv. Robot. Syst.* **2013**, *10*, 36.
- (8) Guo, J.; Bamber, T.; Singh, J.; Manby, D.; Bingham, P. A.; Justham, L.; Petzing, J.; Penders, J.; Jackson, M. Experimental Study of a Flexible and Environmentally Stable Electro-adhesive Device. *Appl. Phys. Lett.* **2017**, *111*, 251603.
- (9) Rus, D.; Tolley, M. T. Design, Fabrication and Control of Soft Robots. *Nature* **2015**, *521*, 467–475.
- (10) Fan, F. R.; Tian, Z. Q.; Wang, Z. L. Flexible Triboelectric Generator! *Nano Energy* **2012**, *1*, 328–334.
- (11) Niu, S. M.; Wang, Z. L. Theoretical Systems of Triboelectric Nanogenerators. *Nano Energy* **2015**, *14*, 161–192.
- (12) Wang, Z. L. Triboelectric Nanogenerators as New Energy Technology and Self-Powered Sensors - Principles, Problems and Perspectives. *Faraday Discuss.* **2014**, *176*, 447–458.
- (13) Wang, Z. L.; Chen, J.; Lin, L. Progress in Triboelectric Nanogenerators as a New Energy Technology and Self-Powered Sensors. *Energy Environ. Sci.* **2015**, *8*, 2250–2282.
- (14) Wu, H.; Huang, Y. A.; Xu, F.; Duan, Y. Q.; Yin, Z. P. Energy Harvesters for Wearable and Stretchable Electronics: From Flexibility to Stretchability. *Adv. Mater.* **2016**, *28*, 9881–9919.
- (15) Xu, L.; Bu, T. Z.; Yang, X. D.; Zhang, C.; Wang, Z. L. Ultrahigh Charge Density Realized by Charge Pumping at Ambient Conditions for Triboelectric Nanogenerators. *Nano Energy* **2018**, *49*, 625–633.
- (16) Wang, J.; Wu, C. S.; Dai, Y. J.; Zhao, Z. H.; Wang, A.; Zhang, T. J.; Wang, Z. L. Achieving Ultrahigh Triboelectric Charge Density for Efficient Energy Harvesting. *Nat. Commun.* **2017**, *8*, 88.
- (17) Xi, F. B.; Pang, Y. K.; Li, W.; Jiang, T.; Zhang, L. M.; Guo, T.; Liu, G. X.; Zhang, C.; Wang, Z. L. Universal Power Management Strategy for Triboelectric Nanogenerator. *Nano Energy* **2017**, *37*, 168–176.
- (18) Wang, Z. L. On Maxwell’s Displacement Current for Energy and Sensors: The Origin of Nanogenerators. *Mater. Today* **2017**, *20*, 74–82.
- (19) Ahmed, A.; Hassan, I.; Ibn-Mohammed, T.; Mostafa, H.; Reaney, I. M.; Koh, L. S. C.; Zu, J.; Wang, Z. L. Environmental Life Cycle Assessment and Techno-Economic Analysis of Triboelectric Nanogenerators. *Energy Environ. Sci.* **2017**, *10*, 653–671.
- (20) Zhang, L.; Zhang, B. B.; Chen, J.; Jin, L.; Deng, W. L.; Tang, J. F.; Zhang, H. T.; Pan, H.; Zhu, M. H.; Yang, W. Q.; Wang, Z. L. Lawn Structured Triboelectric Nanogenerators for Scavenging Sweeping Wind Energy on Rooftops. *Adv. Mater.* **2016**, *28*, 1650–1656.
- (21) Wang, Z. L.; Jiang, T.; Xu, L. Toward the Blue Energy Dream by Triboelectric Nanogenerator Networks. *Nano Energy* **2017**, *39*, 9–23.
- (22) Wang, Z. L. Catch Wave Power in Floating Nets. *Nature* **2017**, *542*, 159–160.
- (23) Xu, L.; Pang, Y. K.; Zhang, C.; Jiang, T.; Chen, X. Y.; Luo, J. J.; Tang, W.; Cao, X.; Wang, Z. L. Integrated Triboelectric Nanogenerator Array Based on Air-Driven Membrane Structures for Water Wave Energy Harvesting. *Nano Energy* **2017**, *31*, 351–358.
- (24) Xu, L.; Jiang, T.; Lin, P.; Shao, J. J.; He, C.; Zhong, W.; Chen, X. Y.; Wang, Z. L. Coupled Triboelectric Nanogenerator Networks for Efficient Water Wave Energy Harvesting. *ACS Nano* **2018**, *12*, 1849–1858.
- (25) Pu, X.; Liu, M. M.; Chen, X. Y.; Sun, J. M.; Du, C. H.; Zhang, Y.; Zhai, J. Y.; Hu, W. G.; Wang, Z. L. Ulstretchable, Transparent Triboelectric Nanogenerator as Electronic Skin for Biomechanical Energy Harvesting and Tactile Sensing. *Sci. Adv.* **2017**, *3*, e1700015.
- (26) Wang, J.; Li, S. M.; Yi, F.; Zi, Y. L.; Lin, J.; Wang, X. F.; Xu, Y. L.; Wang, Z. L. Sustainably Powering Wearable Electronics Solely by Biomechanical Energy. *Nat. Commun.* **2016**, *7*, 12744.
- (27) Yang, Z. W.; Pang, Y. K.; Zhang, L. M.; Lu, C. X.; Chen, J.; Zhou, T.; Zhang, C.; Wang, Z. L. Tribotronic Transistor Array as an Active Tactile Sensing System. *ACS Nano* **2016**, *10*, 10912–10920.
- (28) Bu, T. Z.; Xiao, T. X.; Yang, Z. W.; Liu, G. X.; Fu, X. P.; Nie, J. H.; Guo, T.; Pang, Y. K.; Zhao, J. Q.; Xi, F. B.; Zhang, C.; Wang, Z. L. Stretchable Triboelectric-Photonic Smart Skin for Tactile and Gesture Sensing. *Adv. Mater.* **2018**, *30*, 1800066.
- (29) Pang, Y. K.; Li, X. H.; Chen, M. X.; Han, C. B.; Zhang, C.; Wang, Z. L. Triboelectric Nanogenerators as a Self-Powered 3D Acceleration Sensor. *ACS Appl. Mater. Interfaces* **2015**, *7*, 19076–19082.
- (30) Chen, J.; Zhu, G.; Yang, W. Q.; Jing, Q. S.; Bai, P.; Yang, Y.; Hou, T. C.; Wang, Z. L. Harmonic-Resonator-Based Triboelectric Nanogenerator as a Sustainable Power Source and a Self-Powered Active Vibration Sensor. *Adv. Mater.* **2013**, *25*, 6094–6099.
- (31) Chen, X. Y.; Wu, Y. L.; Yu, A. F.; Xu, L.; Zheng, L.; Liu, Y. S.; Li, H. X.; Wang, Z. L. Self-Powered Modulation of Elastomeric Optical Grating by Using Triboelectric Nanogenerator. *Nano Energy* **2017**, *38*, 91–100.
- (32) Zheng, L.; Wu, Y. L.; Chen, X. Y.; Yu, A. F.; Xu, L.; Liu, Y. S.; Li, H. X.; Wang, Z. L. Self-Powered Electrostatic Actuation Systems for Manipulating the Movement of Both Microfluid and Solid Objects by Using Triboelectric Nanogenerator. *Adv. Funct. Mater.* **2017**, *27*, 1606408.
- (33) Zhou, T.; Zhang, L. M.; Xue, F.; Tang, W.; Zhang, C.; Wang, Z. L. Multilayered Electret Films Based Triboelectric Nanogenerator. *Nano Res.* **2016**, *9*, 1442–1451.
- (34) Fang, H.; Wu, W. Z.; Song, J. H.; Wang, Z. L. Controlled Growth of Aligned Polymer Nanowires. *J. Phys. Chem. C* **2009**, *113*, 16571–16574.
- (35) Li, H. Y.; Su, L.; Kuang, S. Y.; Pan, C. F.; Zhu, G.; Wang, Z. L. Significant Enhancement of Triboelectric Charge Density by Fluorinated Surface Modification in Nanoscale for Converting Mechanical Energy. *Adv. Funct. Mater.* **2015**, *25*, 5691–5697.

(36) Niu, S. M.; Wang, X. F.; Yi, F.; Zhou, Y. S.; Wang, Z. L. A Universal Self-Charging System Driven by Random Biomechanical Energy for Sustainable Operation of Mobile Electronics. *Nat. Commun.* **2015**, *6*, 8975.

(37) Niu, S. M.; Wang, S. H.; Lin, L.; Liu, Y.; Zhou, Y. S.; Hu, Y. F.; Wang, Z. L. Theoretical Study of Contact-Mode Triboelectric Nanogenerators as an Effective Power Source. *Energy Environ. Sci.* **2013**, *6*, 3576–3583.

(38) Niu, S. M.; Liu, Y.; Chen, X. Y.; Wang, S. H.; Zhou, Y. S.; Lin, L.; Xie, Y. N.; Wang, Z. L. Theory of Freestanding Triboelectric-Layer-Based Nanogenerators. *Nano Energy* **2015**, *12*, 760–774.

(39) Chen, X. Y.; Taguchi, D.; Manaka, T.; Iwamoto, M.; Wang, Z. L. Direct Probing of Contact Electrification by Using Optical Second Harmonic Generation Technique. *Sci. Rep.* **2015**, *5*, 13019.

(40) Kellaris, N.; Venkata, V. G.; Smith, G. M.; Mitchell, S. K.; Keplinger, C. Peano-HASEL Actuators: Muscle-Mimetic, Electrohydraulic Transducers That Linearly Contract on Activation. *Sci. Robot.* **2018**, *3*, eaar3276.

(41) Acome, E.; Mitchell, S. K.; Morrissey, T. G.; Emmett, M. B.; Benjamin, C.; King, M.; Radakovitz, M.; Keplinger, C. Hydraulically Amplified Self-Healing Electrostatic Actuators with Muscle-Like Performance. *Science* **2018**, *359*, 61–65.